Continuum Simulations of Acetylcholine Consumption by Acetylcholinesterase: A Poisson−Nernst−Planck Approach†

Y. C. Zhou,*,‡,§,|| Benzhuo Lu,§,||,⊥ Gary A. Huber,|| Michael J. Holst,‡,§ and J. Andrew McCammon§,||,⊥,#

Department of Mathematics, Center for Theoretical Biological Physics, Howard Hughes Medical Institute, Department of Chemistry and Biochemistry, and Department of Pharmacology, University of California at San Diego, La Jolla, California 92093-0365

Received: June 22, 2007; In Final Form: September 3, 2007

The Poisson−Nernst−Planck (PNP) equation provides a continuum description of electrostatic-driven diffusion and is used here to model the diffusion and reaction of acetylcholine (ACh) with acetylcholinesterase (AChE) enzymes. This study focuses on the effects of ion and substrate concentrations on the reaction rate and rate coefficient. To this end, the PNP equations are numerically solved with a hybrid finite element and boundary element method at a wide range of ion and substrate concentrations, and the results are compared with the partially coupled Smoluchowski−Poisson−Boltzmann model. The reaction rate is found to depend strongly on the concentrations of both the substrate and ions; this is explained by the competition between the intersubstrate repulsion and the ionic screening effects. The reaction rate coefficient is independent of the substrate concentration only at very high ion concentrations, whereas at low ion concentrations the behavior of the rate depends strongly on the substrate concentration. Moreover, at physiological ion concentrations, variations in substrate concentration significantly affect the transient behavior of the reaction. Our results offer a reliable estimate of reaction rates at various conditions and imply that the concentrations of charged substrates must be coupled with the electrostatic computation to provide a more realistic description of neurotransmission and other electrodiffusion and reaction processes.

1. Introduction

As one of the most important neurotransmitters, the cation acetylcholine (ACh) is responsible for the communication between neurons and muscle fibers. This communication occurs at a synapse called the neuromuscular junction (NMJ), where ACh is released from the presynaptic vesicles, diffuses across the synaptic cleft, and is hydrolyzed by acetylcholinesterase (AChE) clusters tethered to the postsynaptic membranes. The timely release of ACh and its consumption by AChE are essential for the communication, and the diffusion of ACh appears to be the rate-limiting step of this highly coordinated process. Various computational models have been developed to simulate this diffusion process, including continuum reaction-diffusion models[1−3] and discrete methods such as Monte Carlo,[3−7] Langevin dynamics, and the popular Brownian dynamics.[4,19] Most continuum models emphasize either the diffusion of ACh in the synaptic cleft or the diffusion and reaction of ACh with the AChE monomer or tetramer. In the former case, a rate coefficient is needed to provide the boundary condition for the diffusion equation at the surface of the enzymes,[2,3] whereas in the latter case a steady-state reaction rate coefficient is derived from the solution of the diffusion equations.[20−24,29] Therefore, an accurate estimate of this rate coefficient is of great importance in the study of neurotransmission.

Analytical results for the reaction rate coefficient are available only for very idealized and limited diffusional systems. Diffusion in realistic biomolecular processes like neurotransmission is always complicated by various interactions among the solvent and the involved reactants, such as solvent-mediated hydrodynamic interactions among reactants and electrostatic interactions in a charged system. Given the dominant effect of electrostatics in driving diffusion at a large range of distances between the reactants, many studies have concentrated on the influence of ionic strength and substrate concentration on the electrostatics, and thus the reaction kinetics. For example, the Coulomb and Lennard-Jones potentials have been integrated into Brownian dynamics simulations[4,19] to study the effect of finite substrate concentrations on the steady-state reaction rate coefficient. Nevertheless, when the reactive region is small compared to the receptor's surface or the substrate concentration is large, it is difficult to obtain the rate coefficient or concentration profile accurately by Brownian dynamics simulations or other discrete methods.[19] For these problems, the continuum description of substrate diffusion based on the Smoluchowski (SMOL) equation[25] provides a proper alternative model, and has been attracting increasing interest.[4,19−24,26−29]

The SMOL equation models the diffusion mediated by electrostatic potential; therefore, its coupling with the Poisson−Boltzmann (PB) equation, the Poisson−Nernst−Planck (PNP) equation, should be able to present a realistic and complete description of the electric field, concentration profile, and diffusional flux. Most recent studies[20−24] merely implemented a *partially* coupled system of SMOL and PB equations. In these studies, an electrostatic potential precalculated from the linear or nonlinear Poisson−Boltzmann equation is supplied to the

† Part of the "James T. (Casey) Hynes Festschrift".

* Author to whom correspondence should be addressed. Fax: 1 858 534-4974. Electronic mail: yozhou@math.ucsd.edu.

‡ Department of Mathematics.

§ Center for Theoretical Biological Physics.

|| Howard Hughes Medical Institute.

⊥ Department of Chemistry and Biochemistry.

Department of Pharmacology.

10.1021/jp074900e CCC: $40.75
Published on Web 12/05/2007

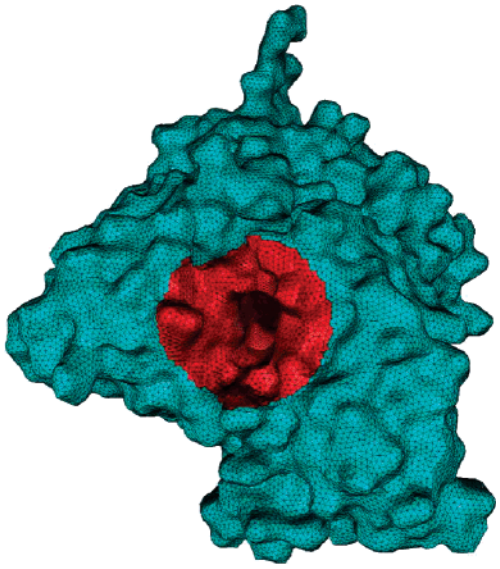

Figure 1. Triangulated molecular surface with reactive site highlighted in red.

SMOL equation to drive the diffusion of substrates, while the concentration profile of these charged diffusing substrates does not contribute to the electrostatic potential. It is interesting that a considerable variation of reaction rates with ionic strength has been found in these studies, which suggests that a further coupling of the diffusing charged substrate with the electrostatic potential through the PNP model might provide new insight into the kinetics of diffusion-influenced reactions. Indeed, the consistence of decoupled and coupled electrodiffusion models has been studied in investigating the permeation of ion channels and enzyme kinetics,[5−9] and the ability of PB theory to estimate the electrostatic potential energy in ion channel has been challenged,[14−17] especially when the size of ions is comparable to the dimension of ion channels.[13,18] We have recently developed a numerical frame for solution of the PNP equations using a hybrid finite element/boundary element approach,[29] which was designed for study of diffusion-reaction events in biomolecular systems. In that work, some examples were performed for reaction rate coefficient calculations in steady-state for simple sphere models, and the results illustrated a strong dependence of the rate coefficient on (charged) substrate concentration.[29] The aim of this paper, then, is a systematic examination of the dependence of the rate coefficient on ionic strength and substrate concentration in biomolecular system, specifically for ACh consumption process by AChE. The transient behavior is also studied.

It is noted that a full coupling of the SMOL equation and the Poisson or Poisson−Boltzmann equation has been implemented in studies of semiconductor devices,[10−12] ion diffusion at charged interfaces[27] and ion transport through lipid membranes,[30,31] where the models are referred to as drift diffusion equations, Smoluchowski−Poisson−Boltzmann (SPB), Nernst−Planck (NP) or Poisson−Nernst−Planck equations (PNP). Although the model in this work will be referred to as PNP, the constituent equations may be varied to achieve the best performance in terms of model accuracy and computational efficiency.

The paper is organized as follows. In section 2 we present our PNP models for the steady-state problem and the time-dependent problems, respectively. The redistribution of ions due to the additional substrates is neglected in the latter to accelerate the computational simulation while otherwise maintaining the model's accuracy. Our newly developed finite element/boundary element hybrid numerical algorithm will also be briefly introduced. In section 3 our PNP models are used to compute the steady-state rate coefficient of ACh consumption by the AChE monomer, and also to study the transient behavior of AChE consumption. The results are discussed and compared with available experimental data and previous simulations to examine the necessity for coupling the substrate concentration with the PNP model. Section 4 concludes our studies with a number of final remarks.

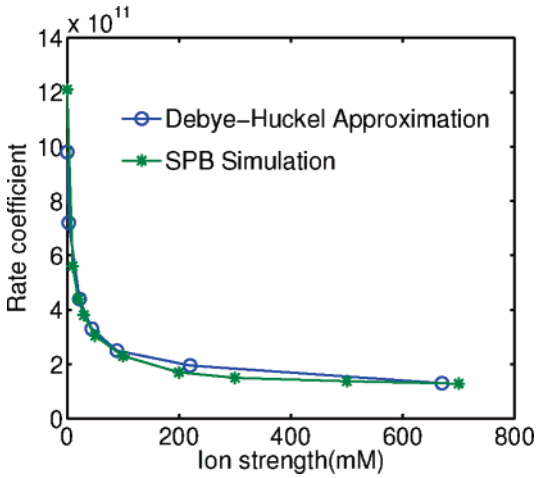

Figure 2. Comparison of reaction rate coefficients (M^{-1} min^{-1}) computed with SPE and fit to the Debye−Hückel law.[36]

2. Models and Methods of Simulation

The diffusion of particles in a potential field under overdamped velocity relaxation conditions is described by the Smoluchowski equation.[25] For steady-state problems, the SMOL equation is coupled with the Poisson equation, which describes the electric field induced by fixed charges in the AChE monomer, the mobile ions, and charged diffusing substrates:

$$\nabla\cdot(D_j(x)e^{-\beta q_j\phi(x)}\nabla(e^{\beta q_j\phi(x)}C_j(x))) = 0 \quad (1)$$

$$\nabla\cdot(\epsilon\phi(x)) = \sum_i q_i\delta(x - x_i) + \sum_j q_jC_j \quad (2)$$

where $D_j(x)$ is the diffusion coefficient for jth ion or substrate with charge q_j and concentration $C_j(x)$, $\beta = 1/(k_BT)$ is the inverse Boltzmann energy, k_B is the Boltzmann constant, T is the absolute temperature, $\phi(x)$ is the electrostatic potential, ϵ is the dielectric constant, and q_i is the fixed charge position x_i inside the molecule. To facilitate the presentation we define the flux of diffusive particles

$$J = -D_j(x)e^{-\beta q_j\phi(x)}\nabla(e^{\beta q_j\phi(x)}C_j(x)) \quad (3)$$

In steady-state diffusion studies, the concentration of ion or substrate on the exterior sphere, i.e., the outer boundary of the modeled system, is set to be its bulk concentration. On the molecular surface, a reflecting boundary condition is assumed for the diffusing particles except for the reactive substrate ACh, which experiences an absorbing boundary condition on the reactive patch, i.e., $C_{ACh} = 0$. This vanishing concentration on the reactive surface is due to the fact that the chemical reaction is much faster than the diffusion.

For studies of time-dependent diffusion we assume that initially the AChE and mobile ions are at a state of electrostatic

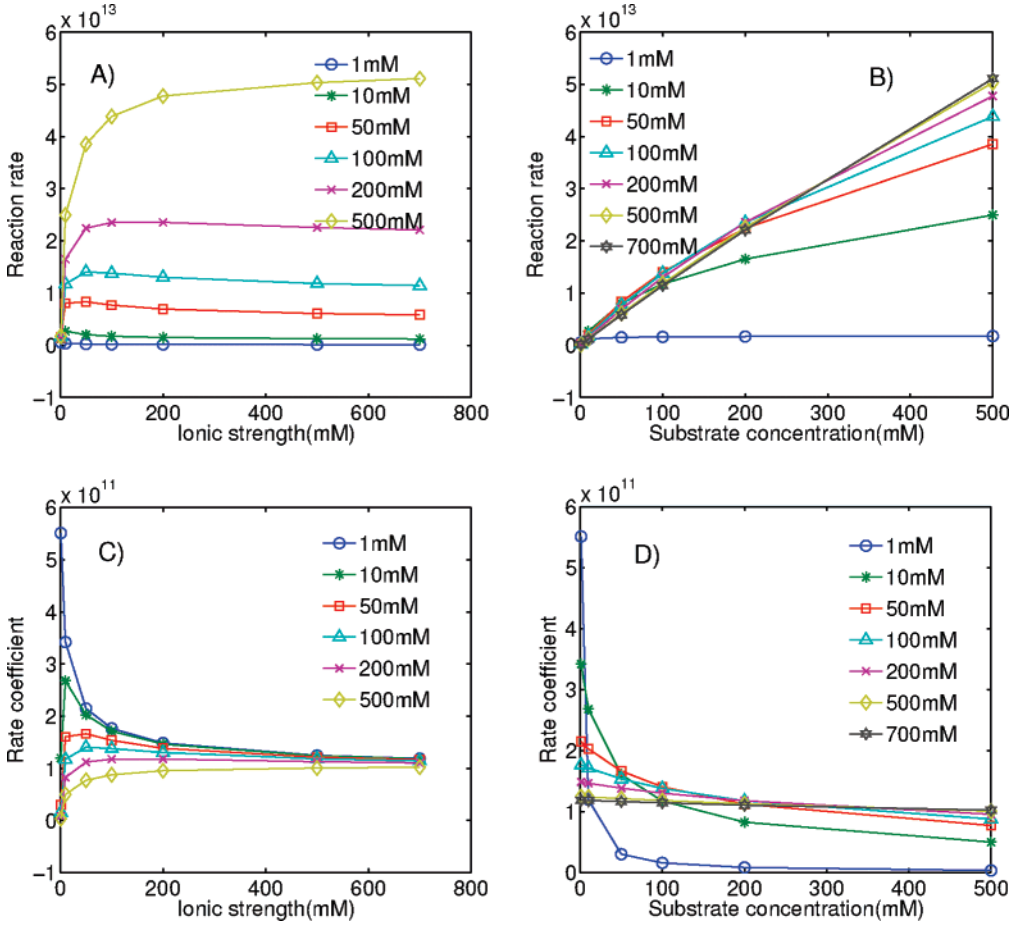

Figure 3. Steady-state reaction rate (min^{-1}) and rate coefficients (M^{-1} min^{-1}) computed with the PNP model. Substrate concentration is not included in calculating the ionic strength.

equilibrium described by the linear Poisson−Boltzmann equation. At $t = 0$, the ACh substrates of a given concentration are released from a sphere away from the AChE monomer. These substrates then diffuse in a large spherical volume surrounding the AChE, and some of them eventually arrive at the reactive molecular surface to be consumed. We note that for this time-dependent problem only the substrates are allowed to diffuse, whereas the concentrations of mobile ions are assumed to always satisfy the Boltzmann distribution. This simplifies the computation; otherwise, two or more time-dependent diffusion equations for mobile ions would also need to be solved. Our time-dependent PNP model thus is given by

$$\frac{\partial C_j}{\partial t} = \nabla\cdot(D_j(x)e^{-\beta q_j\phi(x)}\nabla(e^{\beta q_j\phi(x)}C_j(x))) \quad (4)$$

$$\nabla\cdot(\epsilon\phi(x)) + \kappa^2\phi(x) = \sum_i q_i\delta(x - x_i) + \sum_j q_jC_j \quad (5)$$

where C_j is the concentration of jth substrate and κ is the ionic strength of mobile ions. For both steady-state and time-dependent cases, the electrostatic potential at the exterior sphere is provided by the Debye−Hückel approximation.

In our time-dependent simulations the diffusion starts in a spherical region, which models a ACh-containing vesicle with a radius $r = 240$ Å centered at $(x, y, z) = (0, 480, 0)$. This location is above the AChE active site gorge, which is aligned with the y direction. The exterior boundary is modeled as reflective to simulate a closed box. The other boundary conditions are the same as in the steady-state simulation.

We use our hybrid finite element/boundary element method[29] to solve the PNP equations (1,2) or (4,5). More details on the numerical solution, the boundary conditions, and some examples can be found in ref 29. With our hybrid method the singular component of the electric field induced by the fixed charges inside the molecule is computed with a fast multipole boundary element method,[32] and the regular component of the electric field, and the concentration, are computed with a finite element method.[38] The application of the boundary element method dramatically improves the accuracy of the singular electrostatic component. The regular electrostatic component and the diffusion part of the PNP equations are solved on the same finite element mesh defined on the volume exterior to the AChE; thus, the difficulty of mapping the potential from the regular grids obtained from the APBS electrostatics solver onto the irregular finite element nodes of diffusion is avoided.[20−22]

We use the same molecular structure of AChE as studied in previous work,[20] which is taken from a MD simulation and has a gorge conformation with greater width than the original X-ray structure (1MAH[33]). The wider gorge facilitates the entrance of ACh into the active site. The molecular surface mesh and the entire tetrahedral finite-element mesh are generated using the method described in ref 29. The partial atomic charges and van der Waals radii are taken from the AMBER force-field.[34] It is worth noting that the mesh around the gorge is refined using MSMS,[35] and the overall surface mesh (Figure 1) is relatively finer and smoother than the one used in previous studies. The dielectric constant ϵ is set to 2 inside AChE molecule and 78 in the solvent. The diffusion coefficient D is

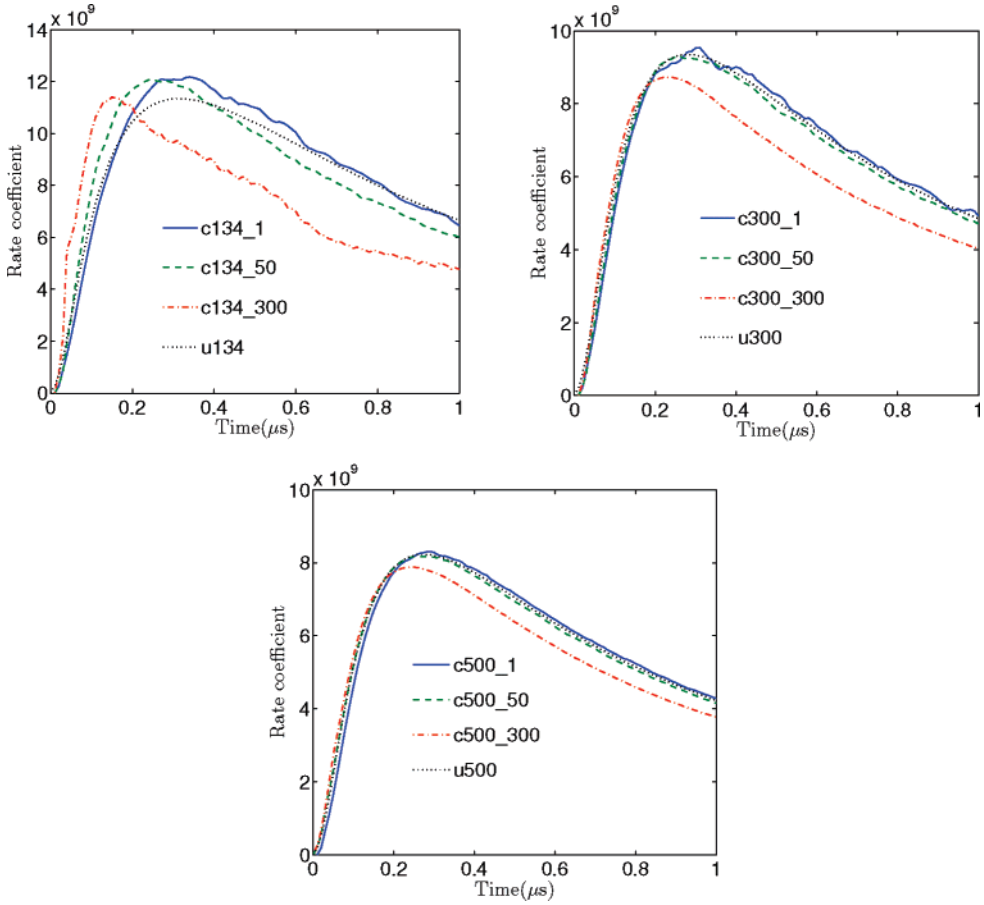

Figure 4. Time-dependent reaction rate coefficients (M^{-1} min^{-1}) normalized by the initial substrate concentration (mM). The ionic strength precedes the underscore and the initial substrate concentration follows the underscore; c represents the PNP model (coupled), and u denotes the SPB model (uncoupled).

chosen to be 78 000 $Å^2/\mu s$, consistent with the previous studies using the SPB model.[20−22,29]

The computational domain is described as follows. A large sphere is chosen to model the far-field boundary of the system. The radius of this exterior sphere is 400 Å for steady-state diffusion and 3000 Å for the time-dependent problem, respectively. The center of this sphere coincides with the geometric center of the AChE monomer, which is taken as the origin of the coordinate system.

3. Results and Discussion

3.1. Steady-State Simulations. The steady-state simulations are conducted at ionic strengths ranging from 0 to 700 mM and the substrate concentration ranging from 1 to 500 mM, with both the PNP model and the SPB model. The reaction rate υ is defined as the total consumption of substrates on the active molecular surface Γ_a (highlighted in red in Figure 1), and the rate coefficient k is the reaction rate divided by the bulk concentration C^0 of the substrate:

$$\upsilon = -\int_{\Gamma_a} J \cdot n \, ds \qquad k = \frac{\upsilon}{C^0} \tag{6}$$

This work will show that k depends strongly on the substrate concentration, rather than being a constant as assumed in previous studies.

The steady-state SPB model is first solved to check the mesh quality and to generate data for comparison with later PNP simulations. As shown in Figure 2, the rate coefficients agree very well with the Debye−Hückel law and also show considerable improvement over former results.[20,21,29] This stems from the consistency of the Debye−Hückel law with the SPB model because of the assumption of no coupling and also from our finer and smoother mesh and the new algorithm for computing the electrostatic potential.

The strong dependence of the rate coefficient on the ionic strength and substrate concentrations in the PNP calculations is illustrated by the steady-state simulations. In particular, at the low substrate concentration 1 mM, the reaction rate reaches a value of about 1.3×10^{12} min^{-1}, which is very close to the maximum reaction rate for this substrate concentration, at an ionic strength around 80 mM, and then grows at very small rate with a further increase in ionic strength (Figure 3A). At higher substrate concentrations (500 mM, for example), the reaction rate initially increases quickly with the ionic strength. Completely different behaviors of reaction rate are found at different substrate concentrations. When the substrate concentration is lower than 200 mM, the initial increase of the rate with the ionic strength is followed by a decrease. This transition is particularly apparent for substrate concentration of 10 mM and has also been observed in the unit sphere model in our previous work.[29]

When the substrate concentration is small, the self-repulsion of the substrates is very weak, and thus the dynamics of the diffusion is close to that of uncoupled models. For this reason, at low substrate concentration, a slight increase of ionic strength is sufficient to screen the substrate interaction and facilitate the aggregation of these substrates near the reactive site. A larger ionic strength will result in stronger screening of the attraction of substrates to the reactive site, which leads to the decrease of

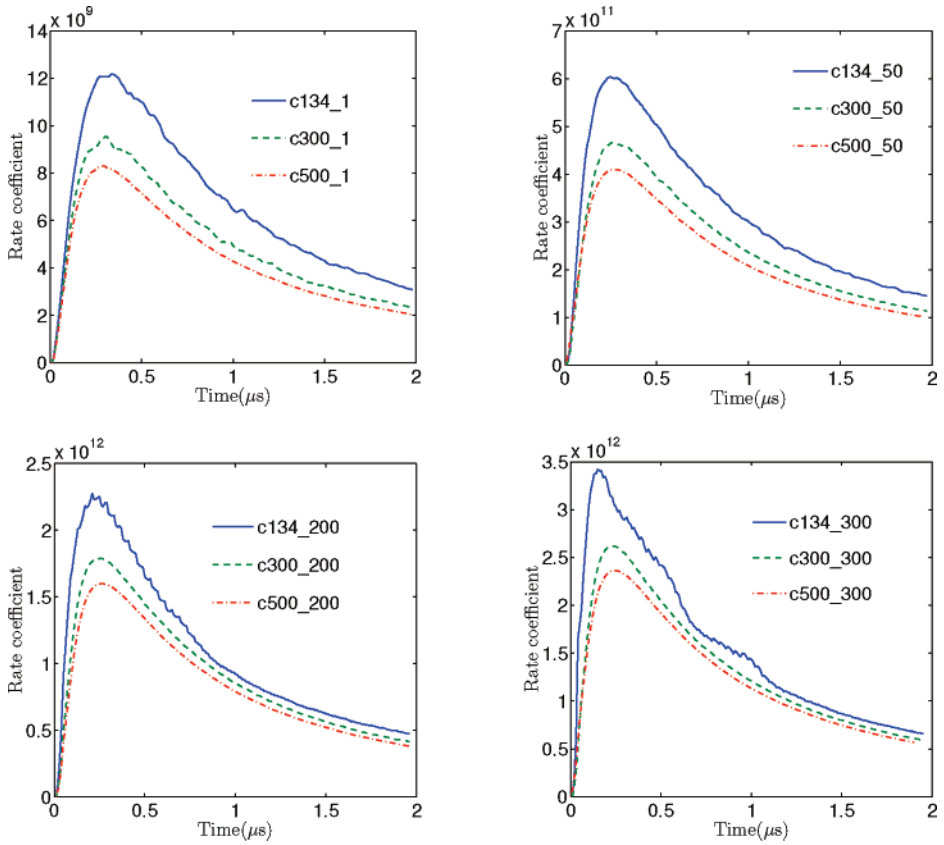

Figure 5. Time-dependent reaction rate coefficients (M^{-1} min^{-1}) computed with PNP model at various ionic strengths. The ionic strength precedes the underscore, and the initial substrate concentration follows the underscore.

reaction rate. On the other hand, a high ionic concentration is necessary to screen the stronger self-repulsion of highly concentrated substrates, which suggests that the increase of ionic strength tends to result in an increase of reaction rate, although the increase in rate becomes less as the ionic strength becomes large. These relations can also be seen from chart B of Figure 3 where the reaction rates are plotted against the substrate concentrations at different ionic strengths. Low ionic strengths are sufficient to screen the self-interaction of substrates only at low substrate concentrations, whereas high ionic strengths are able to facilitate the aggregation and reaction of highly concentrated substrates.

Charts C and D of Figure 3 show the rate coefficients as functions of ionic strength and substrate concentrations, respectively. At the low substrate concentration of 1 mM, the rate coefficient decreases with an increase of ionic strength, and at sufficiently high substrate concentrations the rate coefficient appears to be increasing. Nevertheless, for substrate concentrations between 10 and 100 mM, the rate coefficient initially increases with ionic strength and then gradually decreases to a constant. On the other hand, as mentioned above, for all ionic strengths it is clear from chart C and chart D that the rate coefficient decreases with substrate concentration. The rate coefficient decreases faster at low ionic strengths than at high ionic strength. In particular, both chart C and chart D show that a rate coefficient independent of the substrate concentration can only be found at ionic strengths larger than 500 mM, which is much larger than physiological ion concentrations.

In general, the flux of substrate on the reactive boundary is affected by the balance between the ionic screening effect and inter-substrate repulsion. Our previous numerical results on the charged sphere[29] and the present AChE simulations show that the pure electrostatic repulsion between substrates tends to lower the reaction rate. This observation is different from the conclusion made in a former Brownian dynamics simulation work,[4] where only two substrate concentrations were tested, which may not be completely sufficient to fully explore the influence of substrate concentration on the reaction rate. However, these Brownian dynamics simulations did consider the van der Waals interactions among the substrates; the inclusion of these short-range interactions into the PNP model remains an open problem.

The information contained in Figure 3 and the above analysis imply that the rate coefficient in eq 4 varies considerably with substrate concentration at physiological ion concentrations, approaching a constant value only at very high ionic strengths. Chart C in Figure 3 shows that the rate coefficient decreases from 2×10^{11} to 8×10^{10} M^{-1}·min^{-1} when the substrate concentration increases from 1 to 500 mM at an ionic strength of 134 mM. This suggests that in computational simulations of neurotransmission, a reaction rate coefficient depending on the local ACh concentration, instead of a given constant, could be supplied to models of the postsynaptic membrane to give a more realistic description of the local consumption of the substrate ACh.

3.2. Time-Dependent Simulations. The diffusion and reactions *in vivo* are always time dependent; hence, simulations with time-dependent PNP equations are expected to provide more kinetic information than steady-state simulations. Here the reaction rates and rate coefficients are calculated from a series of simulations with different initial substrate concentrations and ionic strength, to investigate the dependence of the transient reaction rate on ionic strengths and substrate concentrations. Figure 4 illustrates the normalized reaction rate coefficients at different ligand concentrations, i.e., the rate coefficients k of eq 6 divided by the initial ligand concentration at the release site. For example, it is apparent that an increase of ionic strength

results in a decrease of the (normalized) reaction rate coefficient, which peaks at around 12×10^9 $M^{-1}\cdot min^{-1}$ at an ionic strength of 134 mM and reduces to about 8×10^9 $M^{-1}\cdot min^{-1}$ at an ionic strength of 500 mM. Additional support for the decrease of the rate coefficient with the increase of ionic strength is provided by Figure 5. This trend can also be found at all other substrate concentrations considered in the time-dependent simulations and is consistent with results from the steady-state simulations.

Figure 4 also shows the dependence of the peak of the rate coefficient on the substrate concentration and ionic strength. At high ionic strength such as 200 or 500 mM, the maximum rate coefficient with PNP simulation is found to be very close to that calculated from SPB simulations, except at high substrate concentrations such as 300 mM. However, a noticeable shift of the peak was found at the physiological ionic strength of 134 mM. In this case the maximum rate coefficient is obtained at 0.31 μs from the SPB simulation, whereas in the PNP simulations the maximum value was located at 0.15 μs. This forward shift of the peak reaction rate is due to the stronger electric field induced by charged substrates, which in turn speeds the diffusion of the substrates away from their initial location. The increase of ionic strength again results in stronger screening of the electrostatic field, which is seen as the smaller forward shift of peak normalized reaction rate coefficient at high ion concentrations. Such shifts might be relevant in interpreting the discrepancy between the simulated slow discharge of neurotransmitter and the optimal duration[1] and also suggests that the electrostatics should ideally be included in neurotransmission models via fully coupled PNP equations.

4. Conclusion

The Poisson−Nernst−Planck (PNP) equations have been utilized to simulate the steady-state and transient diffusion and reaction of ACh substrates with the AChE monomer. The numerical solution of the PNP equations was conducted with a recently developed hybrid finite element/boundary element method.[29] The results of the PNP models were compared with those of the SPB model, with emphasis placed on the effects of ionic strength and substrate concentration on the reaction rate and rate coefficient for steady-state and transient cases. Strong dependence of the reaction rate on the ionic strength and substrate concentration was found. At high substrate concentrations the steady-state reaction rate coefficient increases with ionic strength. As ionic strength increases, the rate coefficient decreases at low substrate concentrations but increases for high substrate concentrations, and approaches a constant value at a sufficiently large ionic strengths. At physiological ionic strength, the peak of the reaction rate coefficient advances in time as the substrate concentration increases. These considerable variations of rate coefficients at a wide range of ionic strengths suggest that a fully coupled PNP model is desirable to model the electrostatic-driven diffusion and substrate consumption of this system. Therefore, a rate coefficient which depends on both the ionic strength and substrate concentrations should ideally be computed from a PNP model and used as an input to larger-scale neurotransmission simulations.

Acknowledgment. This work is supported in part by the NIH, NSF, the Howard Hughes Medical Institute, National Biomedical Computing Resource, the NSF Center for Theoretical Biological Physics, SDSC, the W. M. Keck Foundation, and Accelrys, Inc.

References and Notes

(1) Khanin, R.; Pamas, H.; Segel, L. *Biophys. J.* **1994**, *67*, 966.
(2) Smart, J. L.; McCammon, J. A. *Biophys. J.* **1998**, *75*, 1679.
(3) Tai, Kaihsu; Bond, S. D.; MacMillan, H. R.; Baker, N. A.; Holst, M.; McCammon, J. A. *Biophys. J.* **2003**, *84*, 2234.
(4) Senapati, S.; Wang, C. F.; McCammon, J. A. *J. Chem. Phys.* **2004**, *121*, 7896.
(5) Eisenberg, R. S. *J. Membr. Biol.* **1990**, *115*, 1.
(6) Eisenberg, R. S. *J. Membr. Biol.* **1996**, *150*, 1.
(7) Eisenberg, R. S. In *New Developments and Theoretical Studies of Proteins*; Elber, R., Eds.; World Scientific: Singapore, 1996; p 269.
(8) Eisenberg, R. S. *J. Membr. Biol.* **1999**, *171*, 1.
(9) Eisenberg, R. S. In *Channels, Receptors and Transporters*, http://www.biophysics.org/btol/channel.html#5.
(10) Selberherr, S. *Analysis and Simulation of Semiconductor Devices*; Springer-Verlag: New York, 1984.
(11) Jacoboni, C.; Lugli, P. *The Monte Carlo Method for Semiconductor Device Simulation*; Springer-Verlag: New York, 1989.
(12) Damocles *IBM Research*, http://www.research.ibm.com/DEMOCLES/home.html.
(13) Roth, R.; Gillespie, D. *Phys. Rev. Lett.* **2005**, *95*, 247801.
(14) Corry, B.; Kuyucak, S.; Chung, S. H. *J. Gen. Physiol.* **1999**, *114*, 597.
(15) Im, W.; Roux, B. *J. Mol. Biol.* **2002**, *319*, 1177.
(16) Corry, B.; Kuyucak, S.; Chung, S. H. *Biophys. J.* **2000**, *78*, 2349.
(17) Moy, G.; Corry, B.; Kuyucak, S.; Chung, S. H. *Biophys. J.* **2000**, *78*, 2364.
(18) Boda, D.; Nonner, W.; Valisko, M.; Henderson, D.; Eisenberg, B. *Biophys. J.* **2007**, *93*, 1960.
(19) Dzubiella, J.; McCammon, J. A. *J. Chem. Phys.* **2005**, *122*, 184902.
(20) Song, Y. H.; Zhang, Y. J.; Shen, T. Y.; Bajaj, C.; McCammon, J. A.; Baker, N. A. *Biophys. J.* **2004**, *86*, 2017.
(21) Song, Y. H.; Zhang, Y. J.; Bajaj, C.; Baker, N. A. *Biophys. J.* **2004**, *87*, 1558.
(22) Zhang, D.; Suen, J.; Zhang, Y.; Song, Y.; Radić, Z.; Taylor, P.; Holst, M.; Bajaj, C.; Baker, N. A.; McCammon, J. A. *Biophys. J.* **2005**, *88*, 1659.
(23) Cheng, Y.; Suen, J.; Radić, Z.; Bond, S. D.; Holst, M.; McCammon, J. A. *Biophys. Chem.* **2007**, *127*, 129.
(24) Cheng, Y.; Suen, J.; Zhang, D.; Bond, S. D.; Zhang, Y.; Song, Y.; Baker, N. A.; Bajaj, C.; Holst, M.; McCammon, J. A. *Biophys. J.* **2007**, *92*, 3397.
(25) Smoluchowski, M. V. *Z. Phys. Chem* **1917**, *92*, 129.
(26) Cohen, H.; Colley, J. W. *Biophys. J.* **1965**, *5*, 145.
(27) Chan, Derek Y. C.; Halle, B. *Biophys. J.* **1984**, *46*, 387.
(28) Zhou, H. X. *J. Phys. Chem.* **1990**, *94*, 8794.
(29) Lu, B.; Zhou, Y. C.; Huber, G.; Bond, S. D.; Holst, M.; McCammon, J. A. *J. Chem. Phys.* **2007**, *127*, 135102.
(30) Nonner, W.; Eisenberg, B. *Biophys. J.* **1998**, *75*, 1287.
(31) Kurnikova, M. G.; Coalson, R. D.; Graf, P.; Nitzan, A. *Biophys. J.* **1999**, *76*, 642.
(32) Lu, B.; Cheng, X.; Huang, J.; McCammon, J. A. *Proc. Natl. Acad. Sci. U.S.A.* **2006**, *103*, 19314.
(33) Bourne, Y.; Taylor, P.; Marchot, P. *Cell* **1995**, *93*, 503.
(34) Cornell, W. D.; Cieplak, P.; Bayly, C. I.; Gould, I. R.; Merz, K. M.; Ferguson, D. M.; Spellmeyer, D. C.; Fox, T.; Caldwell, J. W.; Kollman, P. A. *J. Am. Chem. Soc.* **1995**, *117*, 5179.
(35) Sanner, M. F.; Olson, A. J.; Spehner, J.-C. *Proc. 11th ACM Symp. Comput. Geom.* **1995**, C5−C6.
(36) Radić, Z.; Kirchhoff, P.; Quinn, D. M.; McCammon, J. A.; Taylor, P. *J. Biol. Chem.* **1997**, *272*, 23265.
(37) Stiles, J. R.; Helden, D. V.; Bartol, T. M., Jr.; Salpeter, E. E.; Salpeter, M. M. *Proc. Natl. Acad. Sci. U.S.A.* **1996**, *93*, 5747.
(38) Holst, M. *Adv. Comput. Math.* **2001**, *15*, 139.